Available online at www.sciencedirect.com
ScienceDirect
Geoderma 143 (2008) 261–272
GEODERMA
www.elsevier.com/locate/geoderma

Mapping within-field soil drainage using remote sensing, DEM and apparent soil electrical conductivity

Jiangui Liu [a], Elizabeth Pattey [a,*], Michel C. Nolin [b], John R. Miller [c], Oumar Ka [b]

[a] Agriculture and Agri-Food Canada, Eastern Cereal and Oilseed Research Centre, 960 Carling Avenue, Ottawa, Ontario, Canada K1A 0C6
[b] Agriculture and Agri-Food Canada, Soils and Crops Research and Development Centre, 979 de Bourgogne Avenue, Quebec, Quebec, Canada G1W 2L4
[c] Department of Earth and Space Science and Engineering, York University, Petrie Science Building, 4700 Keele Street, Toronto, Ontario, Canada M3J 1P3

Received 1 March 2007; received in revised form 23 October 2007; accepted 6 November 2007

Abstract

In this study, we evaluated the capability of different datasets for soil drainage mapping within agricultural fields. The evaluated datasets include apparent soil electrical conductivity (ECa), remotely sensed high-resolution airborne hyperspectral reflectance (HR) and C-band synthetic aperture radar (SAR) backscattering coefficients, and a high precision digital elevation model (DEM) generated from GPS measurements. The study site was located in an experimental farm in Ottawa, Ontario, Canada. Three drainage classes representing moderately well drained, imperfectly drained, and poorly drained soils were identified during field surveys according to soil surveyor expert knowledge. Variables that significantly contributed to soil drainage classification were selected from the evaluated datasets with a stepwise discriminant analysis procedure. The selected variables were then used to classify soil drainage with a maximum likelihood classifier. A substantial agreement between the observed and classified drainage classes was achieved using the HR dataset, with a kappa coefficient (κ) of 0.68. Moderate agreement was achieved using the SAR and the ECa datasets, with $\kappa = 0.52$ and 0.55, respectively. The result obtained using the DEM-derived topographic variables showed only a fair agreement ($\kappa = 0.31$). Canonical analysis was also conducted to investigate the association between these datasets and field-observed soil water regime descriptors. This potentially provides an alternative way of drainage mapping using canonical variate. The canonical correlation between the water regime descriptors and the evaluated datasets was 0.81, 0.75 and 0.83 for the HR, SAR and soil ECa datasets, respectively. In this study, the topographic variables were not as efficient, but when combined with the SAR and soil ECa datasets, they improved soil drainage mapping.

Keywords: Soil drainage; Within-field mapping; Remote sensing; Apparent soil electrical conductivity; DEM; Discriminant analysis; Canonical analysis

1. Introduction

Precision agriculture is envisioned as a key approach to increasing the sustainability of crop production; however, traditional soil maps are often not accurate and reliable enough to fulfill the requirements of site-specific crop management. Therefore these soil maps need to be upgraded to finer scales using accurate and objective soil information. Among the various soil properties, soil drainage is important as it directly affects plant growth, water flow and solute transport in soils (Kravchenko et al., 2002). Here, drainage refers to the natural ability of soil to allow water to infiltrate and percolate. Drainage mapping is of interest because soil map users usually need information about soil properties or soil behaviour rather than taxonomic classes for land use and management decision (Bartelli, 1979). Conventionally, soil mapping is made by a trained soil taxonomist to delineate predetermined classes using soil survey along controlled land transects. It is challenging and often problematic to classify a soil concept (e.g., soil drainage class) consistently this way, since the soil classes are frequently overlapping and usually defined by multiple soil properties, and the identification of a soil drainage class relies on the expertise of an individual soil surveyor (Webster and Burrough, 1974). It is

* Corresponding author. Tel.: +1 613 7591523; fax: +1 613 7591724.
E-mail addresses: liu_jiangui@yahoo.com (J. Liu), patteye@agr.gc.ca (E. Pattey).

0016-7061/$ - see front matter.
doi:10.1016/j.geoderma.2007.11.011

also laborious and expensive to map soil drainage at within-field scale through soil survey, because this requires intensive sampling of several representative soil profiles. Thus, methods need to be developed to map soil drainage consistently and inexpensively.

Soil–landscape models have been developed to discriminate soil drainage classes based on topographic variables derived from a digital elevation model (DEM) (Bell et al., 1992, 1994), since there is strong correlation between the shape of the ground surface and the soil drainage characteristics (Troeh, 1964; Acton, 1965). Spatially high resolution and accurate DEM can nowadays be routinely derived from several approaches including stereoscopic techniques using satellite image pairs, synthetic aperture radar (SAR) interferometry, and light detection and ranging (LIDAR) (Abdelfattah and Nicolas, 2002; Toutin, 2004; Liu et al., 2005b). Soil delineation using topographic analysis should benefit from these developments.

Operational measurement of the apparent soil electrical conductivity (ECa) has become the tool of choice in precision agriculture for characterizing the spatial variability of soil properties (Corwin and Lesch, 2005). Since ECa is related with several soil properties, including soil salinity, texture (i.e., clay content), temperature and water content (Corwin and Lesch, 2003; Corwin et al., 2003), it could also be used for soil drainage mapping.

Soil drainage is often related to other soil properties, such as the profile of soil water content and soil texture (Kravchenko et al., 2002), which could be mapped using remote sensing data. In optical remote sensing, the characteristics of the reflectance spectrum from a soil surface are related with soil colour and brightness, as well as other properties, such as soil texture composition, moisture and organic matter content (Huete and Escadafal, 1991; Mattikali, 1997). For instance, soil reflectance was found to change exponentially as a function of volumetric soil moisture (Lobell and Asner, 2002). For microwave remote sensing, the magnitude of radar backscattering from a soil surface is governed by the dielectric constant and soil surface roughness. The dielectric constant in turn, is dependent strongly on soil moisture content and, to a lesser extent, on soil texture composition (Ulaby et al., 1996). Therefore, both optical and radar remote sensing have the potential to map soil properties, such as soil drainage. The advantage of remote sensing techniques over field survey approaches resides in its consistency. Since data may be acquired non-invasively over a large area within a short period of time, with the same sensor configuration and similar environmental conditions.

Remote sensing data have been used for soil drainage classification by several researchers (Lee et al., 1988a,b; Levine et al., 1994; Cialella et al., 1997; Campling et al., 2002). In areas under natural vegetation, the association of vegetation type with soil, or the impact of a soil property on biomass accumulation can be exploited for soil mapping using remote sensing data (Lozano-Garcfa et al., 1991; Korolyuk and Shcherbenko, 1994; Levine et al., 1994). However, in agricultural fields, a number of other disturbing factors, such as management practices, may impact the direct soil-vegetation relationship. Thus, Moran et al. (1997) proposed to use remote sensing data acquired under bare conditions to map agricultural soils. With the development of different remote sensing systems, the opportunity to acquire remote sensing data at an optimal condition will increase.

The objective of this study was to evaluate the relative capability of soil ECa, DEM-derived topographic variables, and high-resolution remote sensing data for mapping within-field soil drainage variability. A maximum likelihood classifier and a discriminant analysis procedure were used for soil drainage classification. In addition, canonical analysis was conducted to investigate the association between the data mentioned above, and the soil information collected from field survey. The feasibility of mapping soil drainage in a continuous manner using canonical variate was discussed. This potentially provides an alternative to soil drainage classification.

2. Materials and methods

2.1. The study site

The study was conducted in two adjacent fields in an experimental farm south of Ottawa, Ontario, Canada (45°18′N, 75°45′W, Fig. 1). The two fields were characterized by seven soil landscape units, with a range of loamy sand to silty clay loam soil texture, a moderately well drained to poorly drained conditions, and a level (0–0.5%) to gently sloping (2 –5%) topography (Marshall et al., 1979). Detailed soil information was introduced in Liu et al. (2005a).

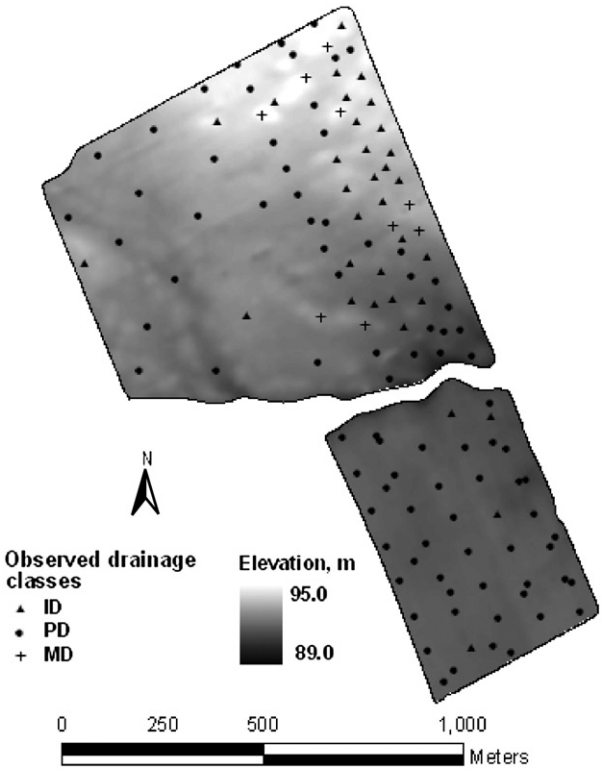

Fig. 1. Elevation map of the study fields showing the locations of the soil sampling sites. Drainage classes are labelled with different symbols; +: moderately well drained (MD); ▲: imperfectly drained (ID); ●: poorly drained (PD). The elevation map was generated using DGPS installed on board of an electrical cart (see text for more details).

2.2. Soil survey and sampling

Intensive soil surveys were conducted in fall 2002 and spring 2005. A total of 144 sites were georeferenced, described and sampled in the two selected fields. Soil drainage classes were determined based on surveyor's knowledge. Of the 144 samples, 9 samples were identified as moderately well drained (MD), 35 as imperfectly drained (ID), and 100 as poorly drained (PD). According to the Canadian Soil Information System (CanSIS; Day, 1982), a soil belongs to MD class if excess surface water is removed somewhat slowly from soil in relation to supply, ID class if water is removed sufficiently slowly to keep the soil wet for a significant part of the growing season, and PD class if water is removed so slowly that the soil remains wet for a comparatively large part of the time when the soil is not frozen. In addition, physical and chemical soil properties were also collected and analyzed for the first 30 cm depth (Perron et al., 2003). The following soil profile information was also recorded *in situ*: depth to a gleyed horizon (D_{Gley}), depth to a contrasting clayed layer (D_{IIC}), and depth to the first C horizon (D_C). Other soil water regime descriptors, such as the wetness index (I_W), the available water capacity within 0 to 50 cm (AWC_{50}) and 0 to 100 cm (AWC_{100}) from surface were also estimated in the laboratory afterwards using pedo-transfer functions mainly based on the morphological datasets (Lavoie et al., 1999). These variables were organized as a database obtained from soil field survey.

2.3. DEM and topographic variables

A DEM was generated with the elevation data collected using a real-time kinematic global positioning system (RTK GPS), with 1 cm vertical accuracy. The GPS sampling density was about 150 points per ha across the fields, with about 13 m interval between transects and 5 m within transects. The point elevation data were interpolated into raster format with an 8×8 m grid size using a block kriging technique implemented in ESRI ArcGIS Geostatistical Analyst (ESRI, 2001). The global trend was modeled and removed from the measured points first, and added back after kriging. Fig. 1 shows the interpolated elevation data, overlaid with soil samples marked with their observed drainage classes. Terrain analysis and simple hydrological functions were used to generate maps of various topographic variables, which include elevation (Z), slope (S), aspect angle (φ), plane (C_{XY}) and profile (C_Z) curvature, convergence index (I_C), compound topographic index (CTI), stream power index (SPI), stream transport index (STI), and specific catchment area (SCA). Detailed formulae used to derive the topographic variables can be found in Hengl et al. (2003).

2.4. Apparent soil electrical conductivity

Soil ECa was measured in November 2002 using a VERIS-3100 instrument within 0–30 cm (ECa_{30}) and 0–100 cm (ECa_{100}) depths. The sampling rate is approximately 150 points per ha, with about 13 m between transects and 5 m within transects. The measured ECa data were also interpolated into 8×8 m grid using the same approach as the DEM. As an example, ECa_{100} is shown in Fig. 2a.

2.5. Remote sensing data

Airborne hyperspectral reflectance (HR) data were acquired with the compact airborne spectrographic imager (CASI) in June 2000 when the fields were bare. Reflectance spectra were measured in 72 bands between 408 and 947 nm with a bandwidth of 7.5 nm and a spatial resolution of 2 m. Initial geometric correction was done using the navigation data recorded onboard

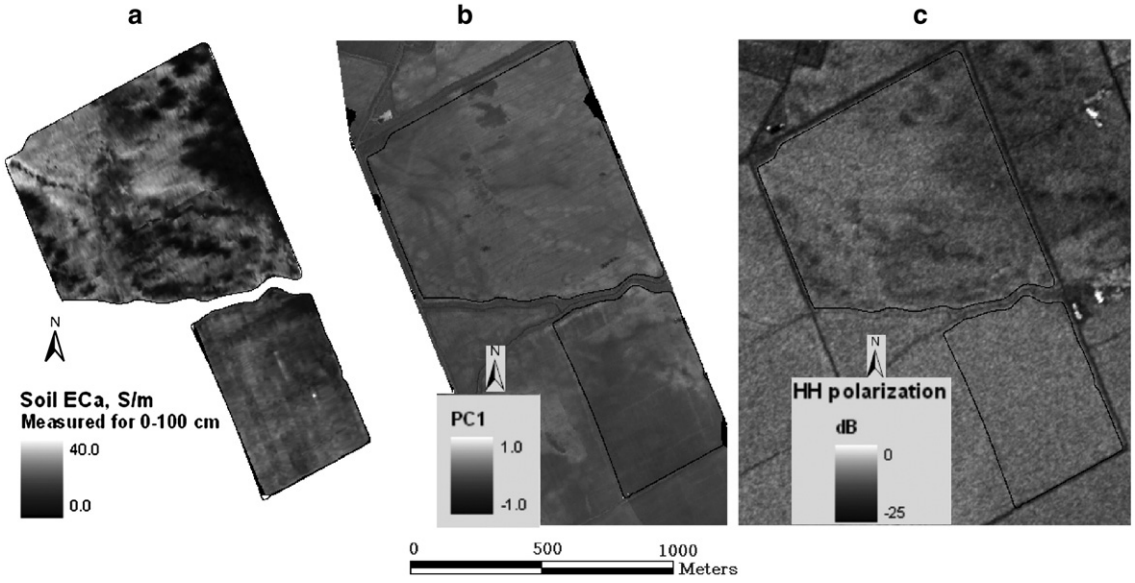

Fig. 2. Maps showing the datasets used in the study: a) the apparent soil electrical conductivity (showing the deeper measurement); b) the principal component of the hyperspectral reflectance (see text, showing the first component); and c) the synthetic aperture radar backscattering coefficient (showing the HH polarization).

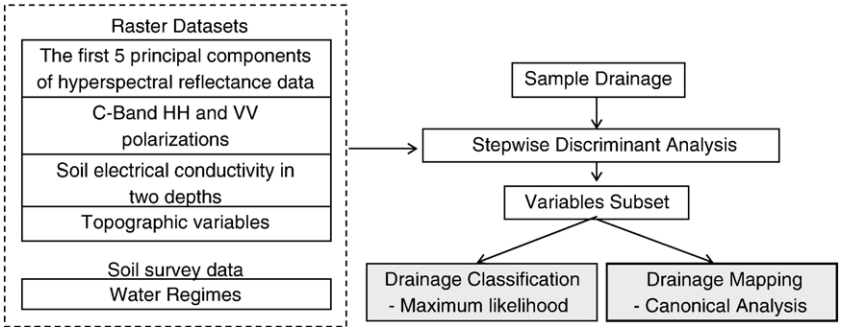

Fig. 3. Schematic of the procedure for analyzing and mapping within-field soil drainage using either the categorical approach by discriminant analysis, or the continuous approach by canonical analysis.

the aircraft. To improve accuracy, a further correction was made using GPS measurements obtained at several ground locations identifiable on the image. The error for geometric correction was below 1 pixel. A principal component (PC) transformation was applied to reduce data dimensionality from 72 to 5. These five PCs, containing over 99.9% of the total variance of the data, were used for subsequent analysis. Image of the first PC is shown in Fig. 2b.

Airborne C-Band SAR polarimetric data were acquired with the CV-580 system in November 2002, at a nominal incidence angle of about 35° at the field centre. The pre-processing of the SAR data, including radiometric calibration and geometric correction, was done by the Canada Centre for Remote Sensing (CCRS). The radiometric accuracy was better than 1 dB. The geocoded image with a pixel size of 4×4 m was also generated in this process (Hawkins et al., 1999). To reduce speckle noise, a Gamma filter with a 5×5 pixel window was applied. SAR backscattering coefficients of the linear HH (horizontally emit and receive) and VV (vertically emit and receive) polarizations were synthesized from the geocoded product using the Polarimetric WorkStation software (Touzi and Charbonneau, 2004). The SAR data was then geometrically registered to the HR image. The accuracy was better than 1 pixel. Image of the backscattering coefficient of the HH polarization is shown in Fig. 2c.

2.6. Discriminant and canonical analyses

As reviewed by McBratney et al. (2003), various geostatistical methods have been developed in digital soil mapping. When denser secondary variables are available to be correlated with the primary soil variable, co-kriging and regression co-kriging are exact estimators for mapping the primary variable. However, they become time consuming and cumbersome if the number of secondary variables is large (Kravchenko et al., 2002). In this study, we used a maximum likelihood classifier based on discriminant analysis to evaluate the capability of different datasets for soil drainage classification. The evaluated datasets include: 1) the hyperspectral reflectance principal components (HR PCs dataset); 2) the C-band SAR backscattering coefficients of the HH and VV polarizations (SAR dataset); 3) soil ECa_{30} and ECa_{100} (ECa dataset); and 4) DEM-derived topographic variables (DEM dataset). In addition, combinations of the HR PCs, SAR and ECa datasets with the DEM dataset were also evaluated to find if DEM could improve drainage classification of these datasets. The soil water regime descriptors obtained from the soil sampling were evaluated for comparison purpose. This approach provides a conventional categorical mapping of soil drainage.

Soil drainage could be more naturally represented with a continuous one-dimensional variable, which can be determined by a few soil water regime descriptors obtained from field surveys. Thus, we used a canonical analysis procedure to explore the association between these water regimes, treated as dependent set, and the HR PCs, SAR, ECa, and DEM datasets, treated as independent sets. A strong canonical correlation would indicate that, the canonical variate derived from the independent dataset reveals soil drainage information, and could be used as a drainage indicator. The canonical variate provides continuous soil drainage mapping, alternative to the conventional categorical mapping. Fig. 3 shows the procedure of the two approaches used in this study.

Topographic variables, soil ECa and remote sensing data were first extracted for each sample site, and joined with the soil survey data to form a soil sample database. A complete list of variables in this database is given in Table 1. The averages, standard deviations, maximum and minimum values of these variables are also given in the table.

Using the sample database, a stepwise discriminant analysis procedure implemented in the SPSS statistics software (SPSS Inc., 1999) was used to select from each dataset a group of variables that significantly contributed to drainage classification. The soil samples were then classified into different drainage classes using the selected variables with a maximum likelihood classifier. Because there is ambiguity in soil class determination, either partial class membership or class probability needs to be considered (Chang and Burrough, 1987). Class probability is represented by the *a posteriori* probability given by:

$$p(k|x) = p(k)p(x|k) / \sum_{i=1}^{c} [p(i)p(x|i)] \quad (1)$$

where x represents a given sample; $p(k)$ and $p(i)$ are *a priori* probability of class k and i, respectively; c is the total number of

Table 1
Descriptive statistics of the variables used in the study

Variable	Mean	Standard deviation	Minimum	Maximum
Soil water regime descriptors (through field survey)				
D_{Gley}(cm)	38.7	14.7	0	90
D_{IIC}(cm)	31.8	34.0	0	130
D_C(cm)	65.8	10.9	40	100
AWC_{50}(cm)	9.9	3.3	4.2	14.3
AWC_{100}(cm)	19.9	5.2	6.9	26.7
I_W(−)	17.4	6.4	2.7	26.7
Topographic variables derived from DEM				
Z(m)	92.6	1.19	90.8	95.4
S(°)	0.33	0.25	0.025	1.34
φ(°)	167	98	1.9	359
C_{XY}(m^{-1})	0.00	0.0003	−0.0009	0.0014
C_Z(m^{-1})	0.00	0.0003	−0.0008	0.0014
I_C(−)	−0.67	15.5	−54.4	84.6
SPI (−)	0.736	2.363	0.0009	22.3
STI (−)	0.059	0.065	0.0005	0.38
SCA (m)	3.85	1.15	1.73	7.94
CTI (−)	8.97	1.57	6.01	14.55
Apparent soil electrical conductivity				
ECa_{30}(S m^{-1})	10.5	7.4	0.8	23.4
ECa_{100}(S m^{-1})	17.7	9.5	0.8	36.3
Principal components of hyperspectral reflectance data				
PC1 (−)	0.056	0.165	−0.278	0.341
PC2 (−)	0.042	0.099	−0.120	0.241
PC3 (−)	−0.015	0.026	−0.088	0.028
PC4 (−)	−0.006	0.017	−0.052	0.032
PC5 (−)	0.0003	0.014	−0.025	0.028
Polarizations of synthetic aperture radar data				
HH (dB)	−11.3	2.1	−17.6	−7.0
VV (dB)	−11.5	1.8	−16.8	−7.3

Note: D_{Gley}, Gley depth; D_{IIC}, depth to a contrasting clayed layer; D_C, depth to the first C horizon; AWC_{50} and AWC_{100}, soil available water capacity within 0–50 cm and 0–100 cm, respectively; I_W, wetness index; Z, elevation; S, slope; φ, aspect angle; C_{XY}, plane curvature; C_Z, profile curvature; I_C, convergence index; SPI: stream power index; STI: stream transport index; SCA: specific catchment area, applied with logarithmic transformation; CTI: compound topographic index; EC_{a30} and EC_{a100}, apparent soil electrical conductivity within 0–30 and 0–100 cm, respectively; PC1–PC5, the first five principal components of the hyperspectral reflectance data; HH (or VV), horizontal (or vertical) transmission and receiving radar backscattering coefficient.

classes; and $p(x|k)$ is the probability density function of class k. The probability density function is expressed as follows:

$$p(x|k) = \exp\left(-0.5D_M^2\right) / \left[2\pi^{n/2}|\Sigma_k|^{1/2}\right] \quad (2)$$

$$D_M^2 = (x-\mu_k)\Sigma_k^{-1}(x-\mu_k)^T \quad (3)$$

where D_M is the Mahalanobis distance; n is the dimensionality of the feature space; μ_k and Σ_k are the mean vector and the covariance matrix of class k, respectively; Σ_k^{-1} is the inverse of the covariance matrix. The average vectors and the covariance matrices can be estimated from a training sample set. Eq. (1) is used to estimate the *a posteriori* probabilities of a given sample belonging to a class, and the class with the maximum *a posteriori* probability is assigned to the sample.

A group of soil water regime descriptors that significantly contribute to drainage classification were identified from this discriminant analysis procedure. These descriptors, obtained directly from field surveys, were used as drainage indicators. The association between these drainage indicators and the other datasets (e.g., HR PCs, SAR, etc.) was then investigated using the canonical analysis procedure implemented in SPSS. The procedures expressed above are based on the soil sample database. When the classification parameters and the canonical weights are estimated from the sample database, soil drainage can be mapped using the gridded datasets across the whole field.

3. Results

3.1. Discriminant analysis and variable selection

A forward stepwise discriminant analysis procedure was applied. The F value to enter and to remove was set to 1.2 and 1.0, respectively. For each dataset, the selected variables are given in Table 2. The overall classification accuracy and the kappa coefficient (κ) are also given in the table. The accuracy is expressed as the percentage of samples that are correctly identified, and the kappa coefficient is used to account for the chance agreement (Foody, 1992). κ is calculated as:

$$\kappa = (P_0 - P_c)/(1 - P_c) \quad (4)$$

$$P_c = \sum_i P_{1i}P_{2i} \quad (5)$$

where P_0 is the overall accuracy; P_c is the chance agreement between the observed and classified categories; P_{1i} and P_{2i} are proportions of samples that are observed and classified as category i, respectively. Following Landis and Koch (1977), the agreement between the classified and observed categories can be divided into five levels according to the value of κ: 0–0.2, slight agreement; 0.2–0.4 fair agreement; 0.4–0.6: moderate agreement; 0.6–0.8: substantial agreement; and 0.8–1.0: almost perfect agreement.

Table 2
Soil drainage classification results using stepwise discriminant analysis

Datasets	Variables selected	Classification accuracy	κ
1. Soil water regime descriptors	D_{Gley}, AWC_{100}	0.90	0.78‡
2. DEM	S, Z, C_{XY}, CTI	0.70	0.31
3. HR PCs	PC1, PC2, PC3, PC4	0.85	0.68‡
4. HR PCs+DEM	PC1, PC3, PC4, S, C_{XY}, CTI	0.84	0.64‡
5. SAR	HH, VV	0.79	0.52†
6. SAR+DEM	VV, S, C_{XY}	0.84	0.66‡
7. ECa	ECa_{100}	0.79	0.55†
8. ECa+DEM	ECa_{100}, S, C_{XY}	0.84	0.66‡

Note: κ, kappa coefficient; ‡ and † represent respectively a substantial and moderate agreement between the observed and the classified drainage classes; DEM, dataset of the topographic variables; HR PCs, dataset of the hyperspectral reflectance principal components, including the first five components; SAR, dataset of synthetic aperture radar backscattering coefficients, including the HH and VV polarizations; ECa, dataset of the apparent soil electrical conductivity, including measurements at 0–30 cm (ECa_{30}) and 0–100 cm (ECa_{100}). The meanings of the selected variables are given in Table 1.

Two soil water regime descriptors, D_{Gley} and AWC_{100}, were the best in discriminating different drainage classes, followed by the HR PCs, SAR, and ECa datasets. These two water regime descriptors thus could be used as field-observed drainage indicators. Fig. 4 is the categorized scatter-plot of these two descriptors. It shows that soil drainage ability is positively related to D_{Gley}, and negatively related to AWC_{100}. When the overall accuracy was considered, the HR PCs dataset only slightly outperformed the SAR and the ECa datasets. However, when κ was considered, the agreement between the observed and classified drainage classes using HR PCs dataset was substantial (0.68), whereas the agreement obtained using the SAR (0.52) and the ECa (0.55) datasets can only be rated as moderate. The DEM dataset only achieved a fair agreement ($\kappa=0.31$) when used alone, but when it was combined with the SAR and the ECa datasets, the overall classification accuracy increased by 5%, and the kappa coefficient increased by more than 0.1. For the HR PCs dataset, there was no increase in the overall classification accuracy and the kappa coefficient when DEM dataset was combined. Slope and plane curvature were selected when the DEM dataset was combined with the three datasets, except that the compound topographic index was also selected for the HR PCs dataset.

3.2. Cross validation

It should be noted here that the classification accuracy and the kappa coefficient reported in Table 2 could be biased, since all the samples were used for both training and validation. Cross validation was thus conducted by dividing the whole sample set randomly into two groups. One group was used for validation and consisted of 25 samples, and the other group was used for training and consisted of the remaining samples ($n=119$). Using the majority of the samples for training ensured robust estimation of the classification parameters, e.g., the mean class vector and the covariance matrix; however, fewer samples were left for validation, especially the MD samples ($n=9$). To maintain enough samples for both validation and training, the cross validation was iteratively run 15 times, and the 375 validation samples from all the iterations were used to calculate the classification accuracy and the kappa coefficient. Confusion matrices for each dataset as well as the classification accuracy and the kappa coefficient are given in Table 3. The datasets, consisted of the selected variables, are marked with the same number as that in Table 2.

Compared with Table 2, the cross validation, using only part of the samples for training, shows a decreased overall classification accuracy and kappa coefficient. The decrease was the most for the HR PCs dataset (with or without the DEM dataset). A possible reason was because the limited number of training samples relative to the number of selected variables induced inaccurate parameter estimation, hence resulted in lower classification accuracy. This was especially true for MD soils, for which only 9 samples were observed in the field.

The two soil water regime descriptors remain to be the best grouping variables, with an overall classification accuracy of 87% and $\kappa=0.70$, although more MD samples were incorrectly classified. For the DEM dataset, most of ID samples were classified as PD, and the classification accuracy (0.69) and κ (029) were the lowest. When the DEM dataset was combined with the ECa dataset, the classification accuracy increased from 0.72 to 0.84, and κ increased from 0.42 to 0.65. This is a bigger increase compared with the HR PCs and the SAR datasets.

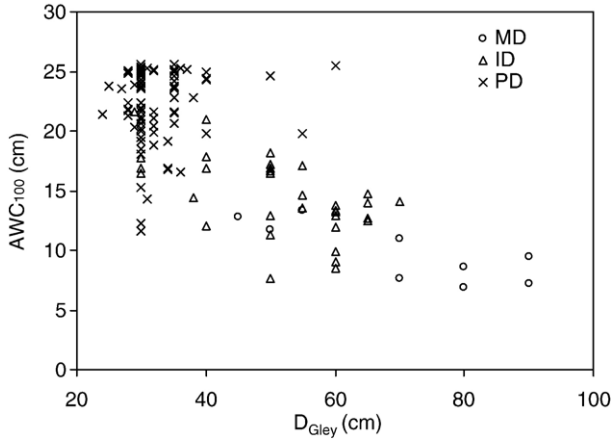

Fig. 4. Scatter-plot between gley depth (D_{Gley}; cm) and available water capacity within the first 100 cm of soil (AWC_{100}), categorized by drainage classes (MD=moderately well drained, ID=imperfectly drained, and PD=poorly drained).

3.3. Within-field drainage classification

From the HR PCs, SAR and ECa datasets, within-field soil drainage classification maps were generated using the maximum likelihood classifier and the variables selected by the stepwise discriminant analysis. The maps are shown in Fig. 5. Classification parameters, including mean vectors, covariance matrices, and *a priori* probabilities of MD, ID and PD soils, were estimated from the whole sample set.

The drainage classification map generated from the SAR dataset appears noisy due to radar speckle. A comparison of the three maps showed that, the proportion of MD soils was the largest for the ECa dataset, and the smallest for the SAR dataset. This could be explained using the classification matrix in Table 3. Classification of the SAR dataset generated a much larger omission error (25 out of 34) than commission error (7 out of 13) for MD class, so the area of this drainage class was underestimated. Whereas the ECa dataset had a much less omission error (9 out of 31) than commission error (46 out of 68) for MD class, thus the area of the MD soils was overestimated. The omission (14 out of 33) and commission (18 out of 37) errors were close for the HR PCs dataset, thus the estimated area of MD soils may be close to the real condition.

3.4. Canonical analysis

Since D_{Gley} and AWC_{100} were observed to be the best soil water regime descriptors for drainage classification, they were used as the dependent dataset in the canonical analysis. The

Table 3
Results from the cross validation of classification

		MD	ID	PD	Accuracy	κ			MD	ID	PD	Accuracy	κ
1	MD	9	15	0			2	MD	16	5	11		
	ID	2	66	15	0.87	0.70‡		ID	2	25	62	0.69	0.29
	PD	0	16	252				PD	6	28	220		
3	MD	19	14	0			4	MD	22	9	2		
	ID	14	49	44	0.74	0.47†		ID	3	56	48	0.76	0.51†
	PD	4	25	206				PD	0	28	207		
5	MD	6	16	9			6	MD	22	5	3		
	ID	6	49	35	0.77	0.48†		ID	2	46	41	0.78	0.52†
	PD	1	18	235				PD	6	24	226		
7	MD	22	9	0			8	MD	24	7	0		
	ID	46	18	26	0.72	0.42†		ID	1	60	29	0.84	0.65‡
	PD	0	25	229				PD	2	22	230		

Note: datasets are marked with the same number as in Table 2, and only comprise the selected variables listed in Table 2; MD, ID, and PD represent moderately well drained, imperfectly drained, and poorly drained soil classes, respectively; the shaded portions are classification matrix; class labels to the left of a matrix represent the observed classes, and that to the top represent the classified classes; κ, the kappa coefficient; ‡ and † represent respectively a substantial and moderate agreement between the observed and the classified drainage classes.

remote sensing (HR PCs and SAR) and the ECa datasets were used as independent datasets. The DEM dataset was not considered independently here, since it was less efficient in drainage classification. However, the combinations of the selected topographic variables with the other three datasets were considered.

Of the two canonical roots calculated, the first root had a significantly higher eigenvalue than the second one for all pairs of datasets; thus, it represented the most significant association between the dependent and independent sets. Results of the canonical analysis are summarized in Table 4. The canonical correlation (R_c), i.e., the correlation coefficient between the canonical variates of the dependent and the independent sets, was high for all the cases, ranging from 0.75 to 0.84. Combining topographic variables with the HR PCs and the SAR datasets slightly increased the canonical R_c, but did not increase that of the ECa dataset. Due to relatively lower loading factors of the topographic variables in the canonical variates, the extracted variance decreased when the topographic variables were included. The percentage redundancy of the independent datasets ranged between 31% and 64%. Given the strong canonical correlation, it is logical to expect that the canonical variates derived from the independent datasets also contain soil drainage information.

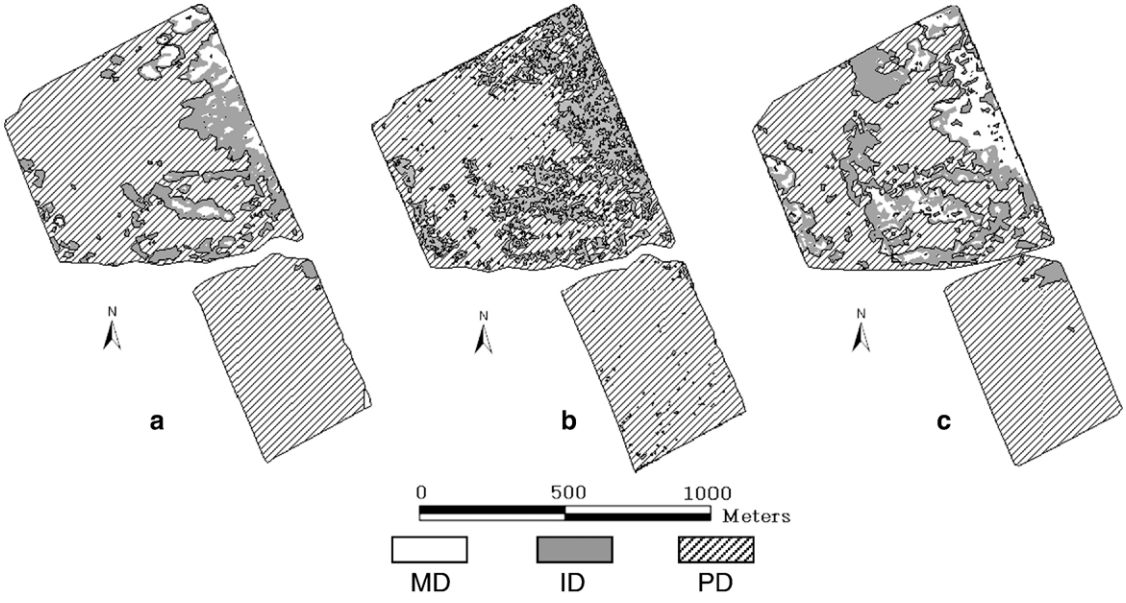

Fig. 5. Within-field soil drainage classification using a) hyperspectral reflectance principal components, b) C-Band SAR linear HH and VV polarizations, and c) apparent soil electrical conductivity measured at 0–30 cm (ECa_{30}) and 0–100 cm (ECa_{100}) depths. MD, ID and PD represent moderately well drained, imperfectly drained and poorly drained soils, respectively.

Table 4
Canonical analyses results

Independent dataset	HR PCs	HR PCs+ DEM	SAR	SAR+ DEM	ECa	ECa+ DEM
R_c	0.81	0.84	0.75	0.77	0.83	0.83
Variance (%)	58	39	90	50	92	52
Redundancy (%)	38	31	50	31	64	38

Note: the dependent set consists of gley depth (D_{Gley}) and available water capacity within 0 to 100 cm depth (AWC_{100}); HR PCs, dataset of the hyperspectral reflectance principal components, including the first five components; SAR, dataset of synthetic aperture radar backscattering coefficients, including the HH and VV polarizations; ECa, dataset of the apparent soil electrical conductivity, including measurements at 0–30 cm (ECa_{30}) and 0–100 cm (ECa_{100}); DEM, dataset of the selected topographic variables from the previous step (Table 2); R_C, canonical correlation.

3.5. Mapping drainage using canonical variates

The canonical weights and the loading factors for the first root are given in Table 5. The loading factor of a variable represents the overall correlation between this variable and the canonical variate. The canonical score (value of a canonical variate) is calculated as $\Sigma(X_i w_i)$, i.e., the weight sum of the variables in the dataset (SPSS Inc., 1999). Here X_i and w_i represent a variable and its canonical weight, respectively.

It can be observed from Table 5 that, for all the cases the loading factors are positive for AWC_{100} and negative for D_{Gley}. Since drainage ability is negatively correlated with AWC_{100} and positively correlated with D_{Gley} (Fig. 4), this means that a lower canonical score of the dependent dataset represents a better drainage condition. It is the same with the canonical score of the independent datasets, since the independent and the dependent datasets are positively associated ($R_c > 0$). Thus the canonical variate derived from the independent dataset serves as an index showing the relative drainage ability. It should be noted that the canonical variates were not calibrated against a single measurable or observed soil variable. Although drainage classes can be defined according to canonical score, this will reduce the information content, since a continuous variable is converted into a variable with only a few nominal values, i.e., drainage classes. To retain detailed information, we thus simply segmented the canonical score into 10 levels, with approximately equal number of pixels in each level. Different levels represent different drainage ability. This is equivalent to histogram equalization to enhance image contrast (Gonzalez and Woods, 2002). Fig. 6a to c are the drainage index maps derived from the segmentation of the canonical variates of the HR PCs, SAR and ECa datasets. A higher value of drainage index in Fig. 6 represents a smaller canonical score and a better drainage condition. This can be confirmed by comparing the drainage index maps in Fig. 6 with the relative classification maps in Fig. 5.

4. Discussions

In the study area, moderately well drained soils are mainly represented by deep (>100 cm) sandy soils with podzolic development and 2–5% slopes terrain. Excess water from spring snowmelt and precipitation is removed somewhat readily in these soils due to the medium to high hydraulic conductivity (15–50 cm h^{-1}). Imperfectly drained soils are developed on shallow (50–100 cm) sandy to coarse–loamy soils over a clayey substratum. The internal soil drainage is restricted by low hydraulic conductivity (<0.5 cm h^{-1}). The poorly drained soils are gleysolic soils with a gentle slope (0–2%) or in depressions. These soils are developed in fine-textured (silty clay loam to silty clay) modified marine materials, with slow internal permeability and surface runoff. Soil drainage strongly determines the available water capacity in the first 100 cm layer (AWC_{100}). In this study, the moderately drained soils have low to moderately low level of available water capacity

Table 5
Canonical weights and loading factors

	Independent set								Dependent set	
HR PCs	PC1	PC2	PC3	PC4	PC5				D_{Gley}	AWC_{100}
Weight	0.20	0.42	0.96	0.59	−0.80				−0.27	0.78
Factor	−0.63	−0.72	0.87	0.90	0.66				−0.86	0.98
HR PCs+DEM	PC1	PC2	PC3	PC4	PC5	S	C_{XY}	CTI	D_{Gley}	AWC_{100}
Weight	0.34	0.53	1.0	0.45	−0.77	0.07	−0.07	0.08	−0.39	0.67
Factor	−0.59	0.66	0.86	0.86	0.62	−0.43	−0.31	0.39	−0.89	0.97
SAR	HH	VV							D_{Gley}	AWC_{100}
Weight	0.52	053							−0.11	0.94
Factor	0.95	0.95							−0.79	0.99
SAR+DEM	HH	VV				S	C_{XY}		D_{Gley}	AWC_{100}
Weight	0.42	0.53				−0.16	−0.15		−0.23	0.82
Factor	0.92	0.92				−0.46	−0.31		−0.84	0.99
ECa	EC_{a30}	EC_{a100}							D_{Gley}	AWC_{100}
Weight	0.15	0.86							−0.12	0.90
Factor	0.92	0.99							−0.80	0.99
ECa+DEM	EC_{a30}	EC_{a100}				S	C_{XY}		D_{Gley}	AWC_{100}
Weight	0.18	0.84				0.06	−0.13		−0.17	0.87
Factor	0.91	0.99				−0.43	−0.27		−0.81	0.99

Note: The meanings of the independent datasets are given in Table 4; the meanings of the variables are given in Table 1.

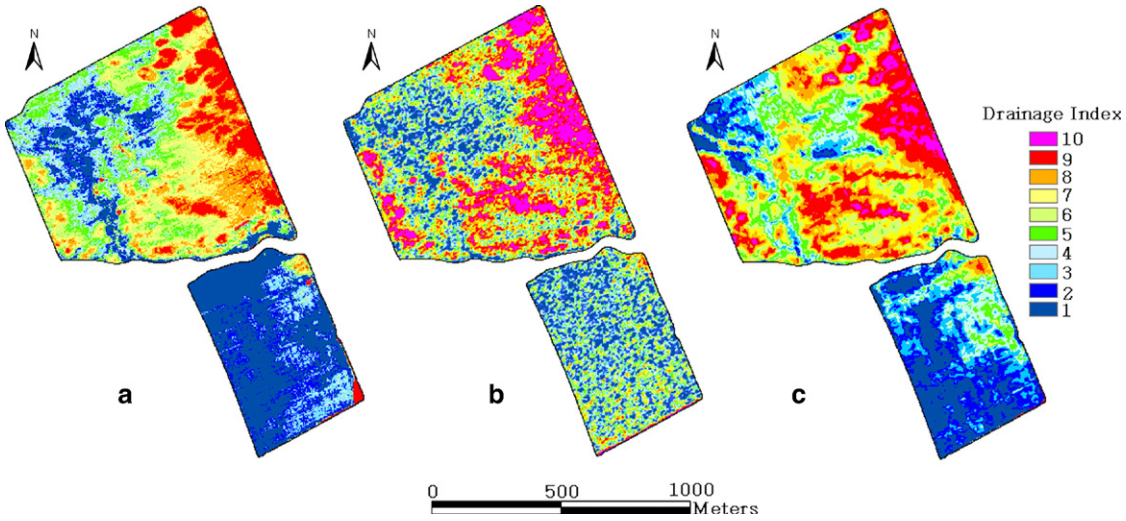

Fig. 6. Within-field soil drainage mapping using canonical variates derived from a) hyperspectral reflectance principal components (HR PCs), b) C-Band SAR linear HH and VV polarizations, and c) apparent soil electrical conductivity within 0–30 cm (ECa_{30}) and 0–100 cm (ECa_{100}) depths. A higher drainage index represents a better drainage condition.

(AWC_{100}=5–10 cm), the imperfectly drained soils have moderate to high available water capacity (AWC_{100}=10–20 cm), and the poorly drained soils have high available water capacity (AWC_{100}>20 cm). Thus AWC_{100} is an important soil drainage indicator. This is consistent with the discriminant analysis results, where both AWC_{100} and D_{Gley} were selected as significant contributors to soil drainage classification. Results from the canonical analysis showed that, the canonical variate derived from the dependent set had a stronger correlation with AWC_{100} than with D_{Gley}, since the absolute loading factor of AWC_{100} was higher than that of D_{Gley} (Table 5).

An investigation of the loading factors of the independent datasets provides some insights to the relationship between the canonical score and the drainage conditions. For the C-band SAR dataset, the loading factors of HH and VV backscattering coefficients were positive (both 0.95). Areas with a better drainage (higher drainage index and smaller canonical score) had lower backscattering values in these two polarizations. This is because radar backscattering coefficient is positively related with soil moisture content (Ulaby et al., 1996), and a better-drained soil is likely to have relative lower level of soil moisture. The loading factors of soil ECa were also positive. Lower moisture content is most likely to induce a lower soil ECa, hence a lower canonical score. It was also noted that ECa_{100} had a higher loading factor, i.e., stronger correlation with soil drainage, than ECa_{30}. The eigen-spectra of the HR PCs dataset are shown in Fig. 7. The curves represent the contribution of each original reflectance channel to the principal components. For instance, PC1 is roughly the average of reflectance in all the bands. A better-drained soil is most likely to have a lower soil moisture content and a higher reflectance, hence a higher PC1 value and a lower canonical score, since PC1 has a negative loading factor of −0.63 (Table 5). PC3 and PC4 have the highest correlation with the canonical variate among the five PCs. It was interesting to note that PC3 received relative small contribution from the near infrared channels, thus represented spectral contrast between the green and red channels.

We have simply used the canonical variates as soil drainage index, with the assumption that the canonical analysis has

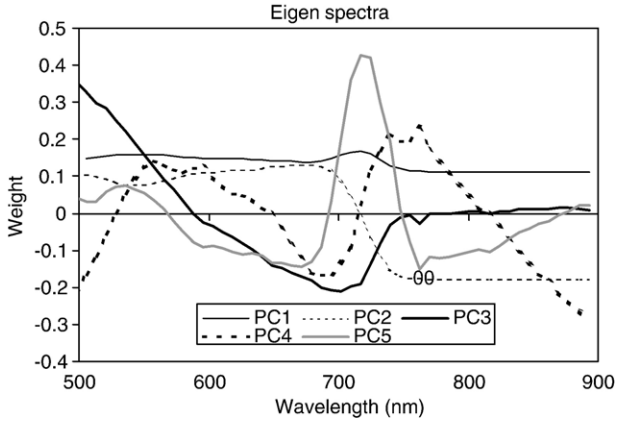

Fig. 7. Eigen-spectra of the first five principal components (PC1–PC5) of the hyperspectral reflectance dataset. The curves show the contribution of each original spectral band to the principal components.

Table 6
Relationship between soil drainage and the canonical variates

	Classification accuracy (%)	κ	MD	ID	PD
HR PCs	80	0.55	<−1.82	−1.82~−0.47	>−0.47
SAR	78	0.52	<−2.15	−2.15~−0.59	>−0.59
ECa	80	0.57	<−2.29	−2.29~−0.52	>−0.52

Note: canonical variates were derived from the HR PCs (hyperspectral reflectance principal components), SAR (HH and VV polarizations), and ECa (soil apparent electrical conductivity at 0–30 cm and 0–100 cm) datasets; MD, ID and PD represent moderately drained, imperfectly drained and poorly drained soils; κ, kappa coefficient.

Table 7
Correlation between AWC_{100} (available water capacity within 0 to 100 cm depth), D_{Gley} (gley depth) and the canonical variates

	AWC_{100}				D_{Gley}			
	a	*b*	R^2	*p*	*a*	*b*	R^2	*p*
HR PCs	4.33	19.45	0.66	<0.001	−11.30	39.14	0.55	<0.001
ECa	4.40	19.45	0.68	<0.001	−10.07	39.14	0.44	<0.001
SAR	3.96	19.45	0.55	<0.001	−9.18	39.14	0.37	<0.001

Note: simple linear regression is used to evaluate the correlation; *a* and *b* are the scale and offset of the linear function; *p* is the statistical significance of the correlation; and R^2 is the coefficient of determinant.

successfully extracted the soil drainage information contained in AWC_{100} and D_{Gley}. It is interesting to investigate the relationship between soil drainage classes and the canonical variates derived from the independent sets. The maximum likelihood algorithm was applied on the canonical variates to assign drainage classes to all the soil samples. The overall classification accuracy, the kappa coefficient, and the data ranges for the three drainage classes are given in Table 6. For instance, if the canonical variate derived from the HR PCs dataset is used for drained classification, an overall accuracy of 80% and kappa coefficient of 0.55 is obtained, representing a moderate agreement between the observed and classified classes. For this canonical variate, a value smaller than −1.82 is assigned to MD, bigger than −0.47 is assigned to ID, and in between −1.82 and −0.47 is assigned to ID. The classification results are comparable with that of the discriminant analysis given in Table 2, with the only exception that the kappa coefficient of the HR PCs dataset is decreased from 0.68 to 0.55. The advantage of the canonical variate is that it is a continuous presentation of soil drainage, which possibly reveals the within-class soil drainage variability.

The relationship between the canonical variate and the two soil water regimes was also investigated. The correlation using a linear regression is summarized in Table 7. In the table, *a* and *b* represent the scale and offset of the linear function using the canonical variate as independent variable. R^2 is the determinant coefficient, and *p* is the significance level. The scale factors show that the canonical variates are positively correlated with AWC_{100}, and negatively correlated with D_{Gley}. Categorized scatter-plot between the water regimes and the canonical variates was shown

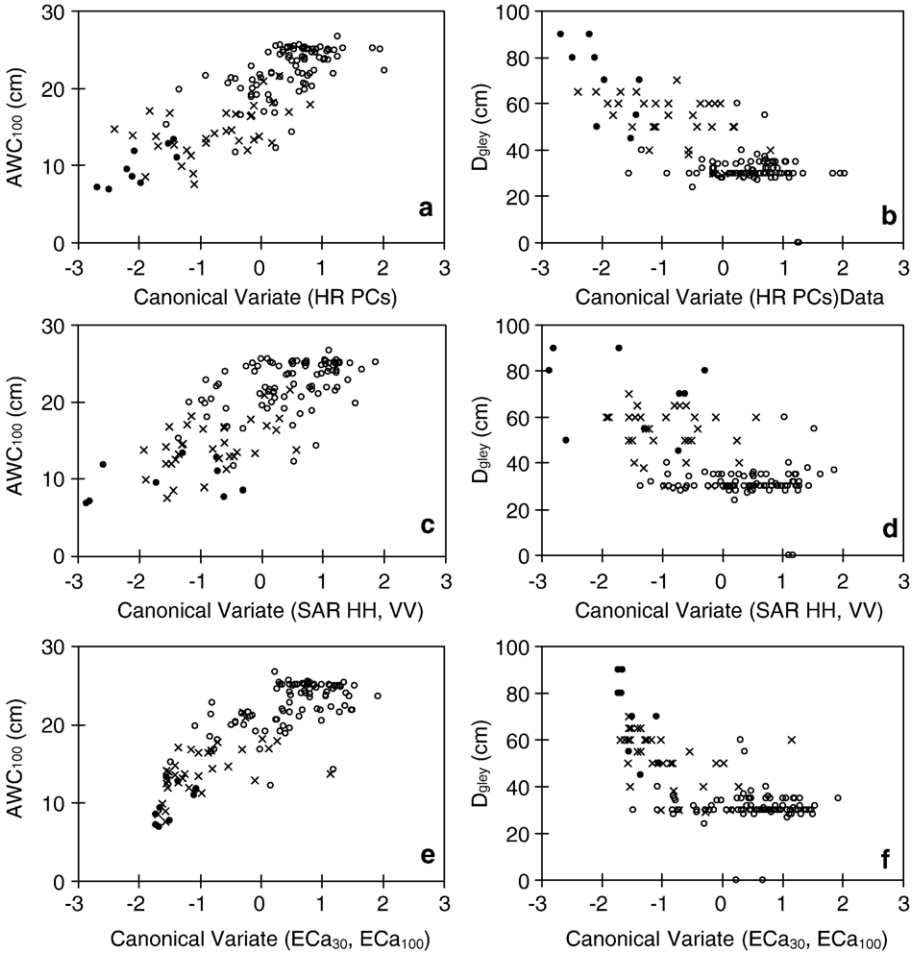

Fig. 8. Categorized scatter-plot between canonical variates and the two water regimes: the available water capacity within 0–100 cm of soil (AWC_{100}; cm) and gley depth (D_{Gley}; cm). The canonical variates are derived from the hyperspectral reflectance principal components (HR PCs), SAR HH and VV polarizations, and soil apparent electrical conductivity within 0–30 cm (ECa_{30}) and 1–100 cm (ECa_{100}). The categories are observed soil drainage classes of moderately well drained (●), imperfectly drained (×), and poorly drained (○) soils.

in Fig. 8. The categories in the figure represent soil drainage class observed from field survey. MD, ID and PD samples are symbolized with dots, crosses and circles, respectively. It is obvious that canonical score increases when soil drainage changes from MD to PD. Although a linear relationship might not be the best to relate the water regimes with the canonical variates, all the relationships are significant at $p < 0.001$ level.

5. Conclusions

The ability of mapping within-field soil drainage conditions using high-resolution hyperspectral reflectance data, C-Band synthetic aperture radar HH and VV polarizations, apparent soil electrical conductivity data, and topographic variables derived from DEM, was evaluated in this study. Two approaches were proposed and tested for soil drainage mapping. The first approach was based on discriminant analysis and maximum likelihood classifier, and the second approach was based on canonical analysis. Categorical and continuous mapping of soil drainage resulted from these two approaches, respectively.

The study showed that, within-field soil drainage could be effectively mapped using high-resolution optical and C-Band radar remote sensing data, and apparent soil electrical conductivity data acquired under bare soil conditions. Topographic variables derived from high-resolution DEM had a lower discriminating ability in this study when used alone. Most probably it is because the study fields are relatively flat with limited variability in the topographic variables. However, when combined with the other datasets, topographic variables could improve drainage classification. The results showed that the sample-lead classification of remote sensing data could be used to predict soil drainage classes. This potentially provides an alternative way to the more traditional soil field survey, which usually requires more resources especially to meet the requirements of precision agriculture. On the other hand, the proposed canonical analysis provides an opportunity to map soil drainage on a continuous basis, revealing the continuous variation of many soil conditions.

The approaches developed in this study were based on ground truthing and statistical analysis rather than on a physical model. The results cannot be applied to a different environment without performing a proper calibration. However, the proposed methodology for mapping detailed soil information using remotely sensed data could be applied to other areas to reduce the effort in field soil surveys. Impacts from other factors, such as vegetation, surface roughness, agriculture land use and variable crop residue conditions were not evaluated, although they could influence the efficiency of mapping soil drainage using remote sensing data. A preliminary stratification procedure should be considered in further study to fully investigate the impact of these agro-environmental factors for soil drainage mapping.

Acknowledgements

The authors would like to acknowledge Dr. N. McLaughlin and S. Burtt for the microtopography data acquisition, Drs. J. Bugden and R. Hawkins for SAR data calibration and processing, Isabelle Perron for her GIS data processing help, and E. Gauthier and L. Lamontagne for their internal review comments. The project was funded by the Canadian Space Agency through a Government Related Initiatives Program (GRIP) and Agriculture and Agri-Food Canada.

References

Abdelfattah, R., Nicolas, J.M., 2002. Topographic SAR interferometry formulation for high-precision DEM generation. IEEE Trans. Geosci. Remote Sens. 40 (11), 2415–2426.

Acton, D.F., 1965. The relationship of patterns and gradient of slopes to soils. Can. J. Soil Sci. 45, 96–101.

Bartelli, L.J., 1979. Interpreting soils data. In: Beatty, M.T., Petersen, G.W., Swindale, L.D. (Eds.), Planning the uses and management of land. American Society of Agronomy, Madison, Wisconsin, pp. 91–116.

Bell, J.C., Cunningham, R.L., Havens, M.W., 1992. Calibration and validation of a soil–landscape model for predicting soil drainage class. Soil Sci. Soc. Am. J. 56, 1860–1866.

Bell, J.C., Cunningham, R.L., Havens, M.W., 1994. Soil drainage class probability mapping using a soil–landscape model. Soil Sci. Soc. Am. J. 58, 464–470.

Campling, P., Gobin, A., Feyen, J., 2002. Logistic modeling to spatially predict the probability of soil drainage classes. Soil Sci. Soc. Am. J. 66, 1390–1401.

Chang, L., Burrough, P.A., 1987. Fuzzy reasoning: a new quantitative aid for land evaluation. Soil Surv. Land Eval. 7, 69–80.

Cialella, A.T., Dubayah, R., Lawrence, W., Levin, E., 1997. Predicting soil drainage class using remotely sensed and digital elevation data. Photogramm. Eng. Remote Sensing 63 (2), 171–178.

Corwin, D.L., Lesch, S.M., 2003. Application of soil electrical conductivity to precision agriculture: theory, principles, and guidelines. Agron. J. 95 (3), 455–471.

Corwin, D.L., Lesch, S.M., 2005. Apparent soil electrical conductivity measurements in agriculture. Comput. Electron. Agric. 46, 11–43.

Corwin, D.L., Lesch, S.M., Shouse, P.J., Soppe, R., Ayars, J.E., 2003. Identifying soil properties that influence cotton yield using soil sampling directed by apparent soil electrical conductivity. Agron. J. 95 (2), 352–364.

The Canada Soil Information System (CanSIS), Manual for describing soil in the field. Revised 1982. In: Day, J.H. (Ed.), Canada Expert Committee on Soil Survey, Agriculture Canada, Research Branch, Land Resource Research Institute. LRRI Contribution no.82-52. Ontario, Ottawa.

ESRI, 2001. Using ArcGis Geostatistical Analyst. GIS by ESRI, Redlands, CA. 300p.

Foody, G.M., 1992. On the compensation for chance agreement in image classification accuracy assessment. Photogramm. Eng. Remote Sensing 58 (10), 1459–1460.

Gonzalez, R.C., Woods, R.E., 2002. Digital Image Processing, 2nd edition. Prentice Hall, Upper Saddle River, New Jersey.

Hawkins, R.K., Touzi, R., Wind, A., Murnaghan, M., Livingstone, C., 1999. Polarimetric Calibration Results & Error Budget for SAR-580 System. Proceedings of CEOS Workshop. Toulouse, France. October 26–29, 1999.

Hengl, T., Gruber, S., Shrestha, D.P., 2003. Digital Terrain Analysis in ILWIS. Lecture notes. International Institute for Geo-Information Science & Earth Observation (ITC), Enschede, Netherlands. pp. 56 URL: http://www.itc.nl/personal/shrestha/DTA/, (Last accessed July 15, 2006).

Huete, A.R., Escadafal, R., 1991. Assessment of biophysical soil properties through spectral decomposition techniques. Remote Sens. Environ. 35, 149–159.

Korolyuk, T.V., Shcherbenko, H.V., 1994. Compiling soil maps on the basis of remotely sensed data digital processing: soil interpretation. Int. J. Remote Sens. 15, 1379–1400.

Kravchenko, A.N., Bollero, G.A., Omonode, R.A., Bullock, D.G., 2002. Quantitative mapping of soil drainage classes using topographical data and soil electrical conductivity. Soil Sci. Soc. Am. J. 66, 235–243.

Landis, J.R., Koch, G.G., 1977. The measurement of observer agreement for categorical data. Biometrics 33, 159–174.

Lavoie, S., Nolin, M.C., Lamontagne, L., Cossette, J.-M., 1999. Atlas agropédologique du sud-est de la plaine de Montréal, Québec.CRDSGC. Extension

Bulletin No. 9. Agriculture and Agri-Food Canada. (http://nlwis-snite1.agr.gc.ca/apaq-aapq/index.phtml?lang=en-CA#).

Lee, K.-S., Lee, G.B., Tyler, E.J., 1988a. Determination of soil characteristics from Thematic Mapper data of a cropped organic–inorganic soil landscape. Soil Sci. Soc. Am. J. 52, 1100–1104.

Lee, K.-S., Lee, G.B., Tyler, E.J., 1988b. Thematic Mapper and digital elevation modeling of soil characteristics in hilly terra. Soil Sci. Soc. Am. J. 52, 1104–1107.

Levine, E.R., Knox, R.G., Lawrence, W.T., 1994. Relationships between soil properties and vegetation at the Northern Experimental Forest, Howland, Maine. Remote Sens. Environ. 47, 231–241.

Liu, J., Miller, J.R., Haboudane, D., Pattey, E., Nolin, M., 2005a. Variability of seasonal CASI image data products and potential application for management zone delineation for precision agriculture. Can. J. Remote Sens. 31 (5), 400–411.

Liu, X., Peterson, J., Zhang, Z., 2005b. High-resolution DEM generated from LiDAR data for water resource management. In: Zerger, A., Argent, R.M. (Eds.), MODSIM 2005 International Congress on Modeling and Simulation. Modeling and Simulation Society of Australia and New Zealand, December 2005. ISBN: 0-9758400-2-9, pp. 1402–1408. http://www.mssanz.org.au/modsim05/papers/liu_x.pdf.

Lobell, D.B., Asner, G.P., 2002. Moisture effects on soil reflectance. Soil Sci. Soc. Am. J. 66, 722–727.

Lozano-Garcfa, D.F., Fernandez, R.N., Johannsen, C., 1991. Assessment of regional biomass–soil relationships using vegetation indexes. IEEE Trans. Geosci. Remote Sens. 29, 331–339.

Marshall, I.B., Dumanski, J., Huffman, E.C., Lajoie, P.G., 1979. Soils, capability and land use in the Ottawa Urban Fringe. Land Resource Research Institute, Research Branch, Agriculture Canada, Ottawa, Ontario. 59 p (http://sis.agr.gc.ca/cansis/publications/on/on47/on47_report.pdf).

Mattikali, N.M., 1997. Soil colour modelling for the visible and near infrared bands of Landsat sensors using laboratory spectral measurements. Remote Sens. Environ. 59, 14–28.

McBratney, A.B., Mendonca Santos, M.L., Minasny, B., 2003. On digital soil mapping. Geoderma 117, 3–52.

Moran, M.S., Inoue, Y., Barnes, E.M., 1997. Opportunities and limitations for image-based remote sensing in precision crop management. Remote Sens. Environ. 61, 319–346.

Perron, I., Nolin, M.C., Pattey, E., Bugden, J.L., Smith, A., 2003. Comparison de l'utilisation de la conductivité électrique apparente (CEa) des sols et des données polarimétriques RSO pour délimiter des unités d'aménagement agricole. 25th Canadian Symposium on Remote Sensing — 11ième Congrès de l'Association québécoise de télédétection. Montréal, Quebec, pp. 14–16. October 2003. CD-ROM.

SPSS Inc., 1999. SPSS for Windows, release 10.0.1. SPSS Inc, Chicago.

Toutin, T., 2004. Comparison of stereo-extracted DTM from different high-resolution sensors: SPOT-5, EROS-A, IKONOS-II, and QuickBird. IEEE Trans. Geosci. Remote Sens. 42 (10), 2121–2129.

Touzi, R., Charbonneau, F.J., 2004. PWS: a friendly and effective tool for polarimetric image analysis. Can. J. Remote Sens. 30 (3), 566–571.

Troeh, F.R., 1964. Landform parameters correlated to soil drainage. Soil Sci. Soc. Am. J. 28, 808–812.

Ulaby, F.T., Dubois, P.C., van Zyl, J., 1996. Radar mapping of surface soil moisture. J. Hydrol. 184, 57–84.

Webster, R., Burrough, P.A., 1974. Multiple discriminant analysis in soil survey. J. Soil Sci. 25, 120–134.